Publications

Available Online

J. Sci. Res. **15** (2), 463-472 (2023)

JOURNAL OF SCIENTIFIC RESEARCH

www.banglajol.info/index.php/JSR

Optimal Efficiency Control of Wind Mill Induction Generator Using Loss Minimization Technique

A. A. M. Faizal*, R. S. Rajam

Department of EEE, V V College of Engineering, Toothukudi District, Tamil Nadu, India

Received 5 October 2022, accepted in final revised form 25 January 2023

Abstract

Improvement of the operating efficiency of generators used in large wind power generation systems becomes important since such a large machine's power loss is not negligible. In the conventional method integral controller is used to reduce the power loss by up to 25 % at low wind speeds. The proposed PID controller method is based on flux level reduction, where the flux level is computed from the machine model for the optimum d-axis current of the generator. For the vector-controlled induction generator, the d-axis current controls the excitation level to minimize generator loss. In contrast, the q-axis current controls the generator torque, by which the speed of the induction generator is controlled according to the variation of the wind speed in order to produce the maximum output power, thereby improve the efficiency of the induction generator.

Keywords: Loss minimization; Wind power generation system; Squirrel cage induction generator; Mosfets.

doi: http://dx.doi.org/10.3329/jsr.v15i2.62111 J. Sci. Res. **15** (2), 463-472 (2023)

1. Introduction

With the ever-increasing demand for power, there is a great interest in developing renewable energy and increasing energy conservation efforts. Because of that, technological research is being directed toward utilizing wind energy. Wind farms are being built owing to the policy of low tariff plans in a greater number of on-shore and off-shore for electricity from natural renewable wind energy sources [1]. According to variable wind velocities, the maximum power capture, it is advantageous to change the rotational speed of the turbine/generator [2,3]. Optimal Tip Speed Ratio (TSR) [4,5] and research-based control [6,7] are two methods for maximum wind power extraction. The optimal TSR method is used for the practical system where wind speed and turbine speed need to be measured. The loss of induction machines is directly related to the choice of flux level [8]. The higher the flux level is, the larger the iron losses are. However, an excessive decrease in the flux causes higher copper losses. There is an optimal flux level that minimizes the machine loss. Since the wind speed is usually lower than the rated

* *Corresponding author*: aamdfaizal@gmail.com

value and the wind turbines run at low speed and hence at light load, the generator flux level can be decreased for core loss reduction, which results in higher system operating efficiency.

Numerous schemes have been proposed concerning the choice of optimal excitation current or flux level for a given operating point [9,10]. The efficiency improvement techniques can be divided into two categories; one is the model-based, and another model is the online power search optimization technique. In the model-based scheme, the loss is expressed in machine parameters depending on load conditions [11,12]. Fast convergence for variable wind speeds is the major advantage of this method. On the contrary, the online power search optimization method continuously varies the flux current component to reach the maximum output power point [13,14]. This method does not require any machine parameter, so it is insensitive to parameter perturbation. However, it is effective only at steady state conditions, even with constant output power. It produces continuous flux and torque pulsations around the optimum operating point. Improving the operating efficiency of generators used in large wind power generation systems becomes important since such a large machine's power loss is not negligible.

For full load conditions, the efficiency of the variable-speed wind power generation system is almost the same as mentioned in [15]. However, the gearbox and the induction generator losses at light load increase. To increase the system efficiency at light load, both the gearbox and generator efficiency should be increased. So far, only a few literatures have been proposed that dealt with the efficiency control of the induction generator in wind power conversion systems [16,17], even though a large number of research results on that of motor drives have been published [18].

In this paper, a new relationship for optimal flux current references according to the variable wind speed is derived based on machine loss equations that minimize the generator's total loss. The derived flux current reference is the function of machine parameters and wind speed. Using this method, up to 25 % of the power loss can be saved at low wind speed, which results in the increase of generator output power.

2. Wind Power Generation System

A wind power generation system for a cage-type induction generator connected with back-to-back PWM converters to the utility grid is discussed in this paper, and it is shown in Fig. 1. Depending on the wind speed, the turbine, and the generator speeds are adjustable, and the full power generated flows into the back-to-back PWM converters. The power captured by the wind turbine is written as described in [18]

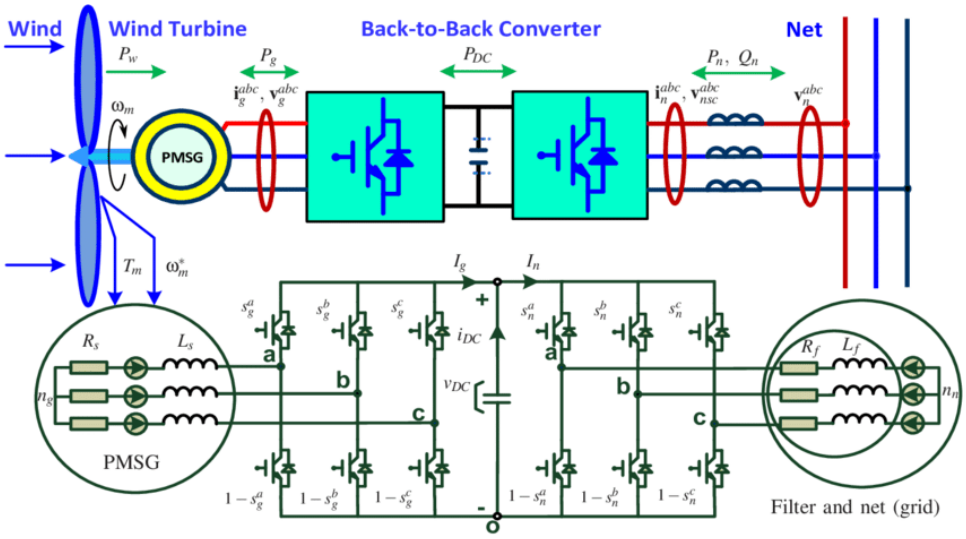

Fig. 1. Back-to-back PWM converter system for grid connection.

$$P_{rot} = \frac{1}{2}\rho\pi R^2 \upsilon^3 C_p(\lambda) \quad (1)$$

and the tip-speed ratio is defined as

$$\lambda = \frac{\omega_r R}{\upsilon} \quad (2)$$

Where,

ρ : specific density of air [kg/m3]; υ : wind speed [m/s];R : radius of the turbine blade [m]; *ωt:* turbine speed;C_p: Coefficient of power conversion.

Fig. 2 shows the characteristics curves of the windmill induction generator. The power captured in the turbine blade is a function of the rotational speed, and the output power is the maximum at the particular rotational speed shown in Figs. 2(a) and (b) show the relationship between the power conversion coefficient and blade tip speed ratio (TSR) that the C_p is the function of λ, and it is the maximum at λ *opt.* Hence, to get the maximum power from the wind, λ should be maintained at λ *opt,* which is determined by the blade design. Then, from Eq. 1 and Eq. 2, the maximum power is as follows

$P_{max} = 0.5\ \rho\pi R^2 C_{p\,max} \upsilon^3$.

The control block diagram of the induction generator is shown in Fig. 3. Once the generator speed reference is determined, the other control structure is the same as that in the induction motor drives.

(3)

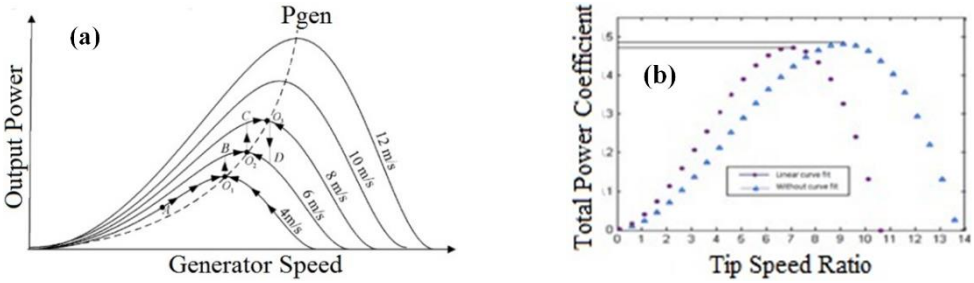

Fig. 2. Characteristic curves of the wind turbine system, (a) output power vs. rotational speed (b) power conversion coefficient vs. tip-speed ratio.

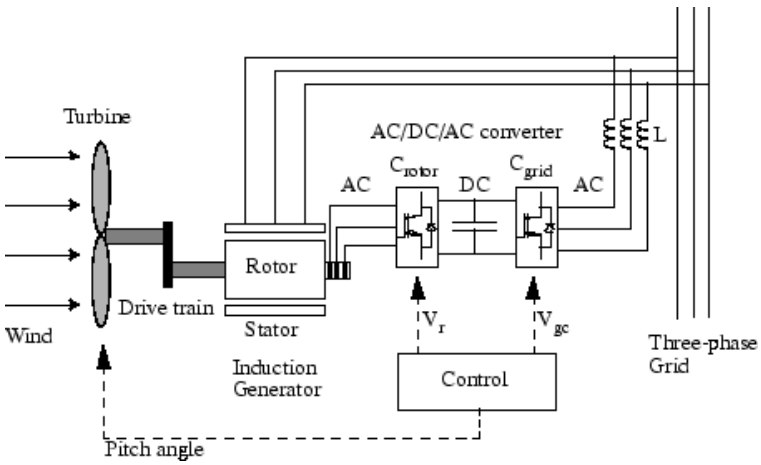

Fig. 3. Control block diagram of induction generator.

3. Loss Minimization Technique

The magnetizing flux can be controlled to reduce the iron loss of the induction machine. This can be achieved by controlling the flux current component i_{ds} in vector control schemes. In the case of an induction generator, the flux current reference is derived as a function of wind speed, which will be described as follows. The d-q equivalent circuits in the synchronous reference frame for the induction machine are shown in Fig. 4, in which a resistance represents the core loss R_{fe}

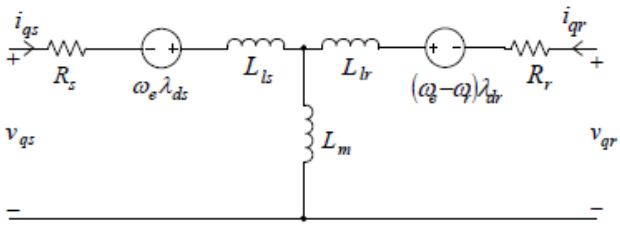

Fig. 4. D-q equivalent circuits of three-phase induction machine.

Neglecting the mechanical loss and stray loss, the loss of the induction machine can be classified into the copper loss and the iron loss as

Stator copper loss :$i_{ds}^2 R_s$+$i_{qs}^2 R_s$Rotor copper loss : $i_{dr}^2 R_r$+$i_{qr}^2 R_r$ (4)

Stator iron loss :$K_h \omega_e \lambda_r^2 + K_e \omega_e^2 \lambda_r^2$Rotor iron loss :$K_h \omega_{sl} \lambda_r^2 + K_e \omega_{sl}^2 \lambda_r^2$ (5)

Where R_s , R_r are the rotor and stator resistances, R_{fe} is the iron loss resistance, i_{ds} , i_{qs} are the d-q stator currents, ω_e is the supply angular frequency, ω_r is the rotor angular frequency, ω_{sl} is the slip angular frequency, λ_r is the rotor flux, K_h , K_e are the coefficients of hysteresis and eddy current losses.

The rotor iron loss is often neglected since the slip frequency is so small at normal operating conditions. The following Eq. 6 and Eq. 7 are the dynamic equations of the induction machine.

$$v_{ds} = i_{ds}R_s - \omega_e \lambda_{qs} + p\lambda_{ds} ; v_{qs} = i_{qs}R_s + \omega_e \lambda_{ds} + p\lambda_{qs}; 0 = i_{dr}R_r + (\omega_e - \omega_r)\lambda_{qr} + p\lambda_{dr} \quad (6)$$

$$0 = i_{qr}R_r - (\omega_e - \omega_r)\lambda_{dr} + p\lambda_{qr}; 0 = i_{dfe}R_{fe} + \omega_e \lambda_{qs} - p\lambda_{dm}; 0 = i_{qfe}R_{fe} + \omega_e \lambda_{ds} - p\lambda_{qm} \quad (7)$$

Where v_{ds} and v_{qs} are the d-q stator voltages, i_{dfe} and i_{qfe} are the d-q currents flowing through R_{fe} , i_{dm} and i_{qm} are the d-q magnetizing currents, λ_{ds} and λ_{qs} are the d-q stator flux linkages, λ_{dm} and λ_{qm} are the d-q magnetizing flux linkages.

The stator d-q current components are expressed as

$$i_{ds} = i_{dm} + i_{dfe} - i_{dr} \;\&\; i_{qs} = i_{qm} + i_{qfe} - i_{qr} \quad (8)$$

The generator torque equation in steady state is given by

$$T_e = \frac{3}{2}\frac{P}{2}(\lambda_{qs} i_{ds} - \lambda_{ds} i_{qs}) \quad (9)$$

Where P is the number of pole pairs. The mechanical power can be expressed as

$$P_m = T_e \omega_m = \frac{P}{2} T_e \omega_r \quad (10)$$

To find a simple mathematical form for the minimum loss condition, the model is to be simplified which is shown in Fig. 5. For this; it is assumed that the leakage inductances can be neglected [17].

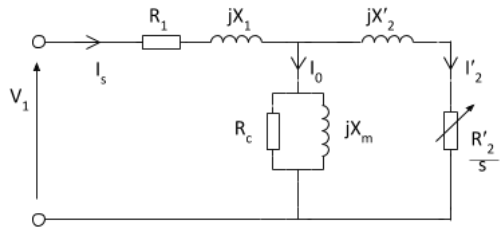

Fig. 5. Simplified d-q equivalent circuit.

The power loss can be expressed as

$$P_{loss} = \frac{3}{2}\left(\frac{L_m^2 \omega_r^2}{R_r + R_{fe}} i_{ds}^2 + R_s (i_{ds}^2 + i_{ds}^2) \frac{R_r R_{fe}}{R_r + R_{fe}} i_{qs}^2\right) \quad (11)$$

To investigate the effects of each current component on the power loss, let's divide Eq. 13 into the two components as

$$P_{loss,d} = \frac{3}{2}\left(R_s + \frac{L_m^2 \omega_r^2}{R_r + R_{fe}}\right) i_{ds}^2 \quad ; \quad P_{loss,q} = \frac{3}{2}\left(R_s + \frac{R_r R_{fe}}{R_r + R_{fe}}\right) i_{qs}^2 \tag{12}$$

The iron loss is decreased by reducing the flux at a given constant torque and speed. The machine flux is reduced by decreasing the d-axis current. Since the torque is proportional to the product of the rotor flux and the stator q-axis current, the q-axis current should be increased in order to maintain the same torque at the reduced rotor flux while the d-axis current decreases, of which tendency is shown in Fig. 6.

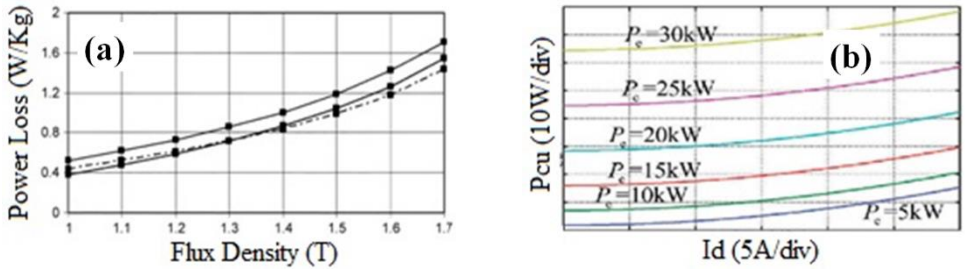

Fig. 6. Induction generator characteristics curve, (a) induction generator loss for different flux levels, (b) power loss curve vs. d-axis current.

To obtain the minimum loss point, Let's take the derivative of the summation of Eq. 12 with regard to the d-axis current and set it to zero,

$$\frac{dP_{loss}}{di_{ds}} = 0 \tag{13}$$

Then, the optimum flux current reference *ids loss_* is obtained as

$$i_{ds\_opt}^4 = \left(\frac{T_e}{K_t}\right)^2 \left(R_s + \frac{R_{fe} R_r}{R_r + R_{fe}}\right) / \left(R_s + \frac{L_m^2}{R_r + R_{fe}} \left(\frac{n \lambda_{opt} v}{R}\right)^2\right) \tag{14}$$

Using Eq. 14, the power loss characteristics with regard to the d-axis current at different wind speeds for the constant torque are drawn in Fig. 6(b), being the wind speed as a parameter. At lower wind speeds, the saving of power loss is more significant than at higher wind speeds, as expected.

4. Simulation of Space Vector PWM and Results

The Space Vector Pulse Width Modulation (SVPWM) MATLAB Simulink model is shown in Fig. 7(a). From the figure, the reference frequency and the reference voltage is given to 3φ sine generator that generates the Vabc FV bus is obtained from the low pass filter, then Vabc & FV bus is given to ab transform that transforms the input voltage to the corresponding signal for ab vector sector.

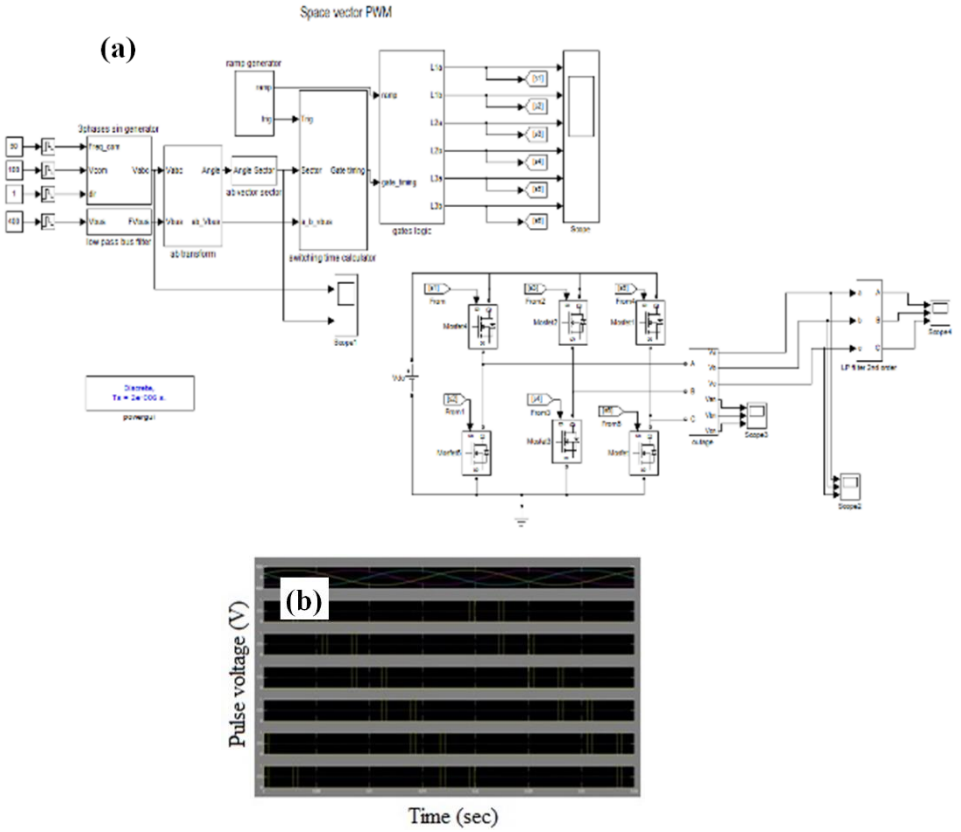

Fig. 7. MATLAB Simulink model of Space Vector Pulse Width Modulation and switching (a) Simulink model of SVPWM, (b) Gating signals of the MOSFET.

The ramp generator and ab angle sec output tor is given to the switch using a time calculator that generates gate timing signal to gates logic. From the gate logic circuit, the corresponding 6 gating signals are given to 6 switches. According to the gating signal of a switch, the inverter operates correctly and produces ac off signal, which is given to a second-order low pass filter to get a pure sine waveform, as shown in Fig. 7(b).

Fig. 8 shows the overall block diagram of the wind turbine control system. The ramp signal and a random number signal are compared, then an error signal is generated called wind speed. Rotor radius, wind speed, and generator speed, the torque of wind turbine is controlled by adjusting β and λ values. Now the generator speed interacts so that i_d ref and i_q ref are transformed into i_r phase, i_y phase and i_b phase values.

SVPWM signal is given to a universal bridge, which acts as a switch where the gate pulse will control the signal and produce a constant DC. SVPWM directly transforms the stator voltage vectors into PWM signals.

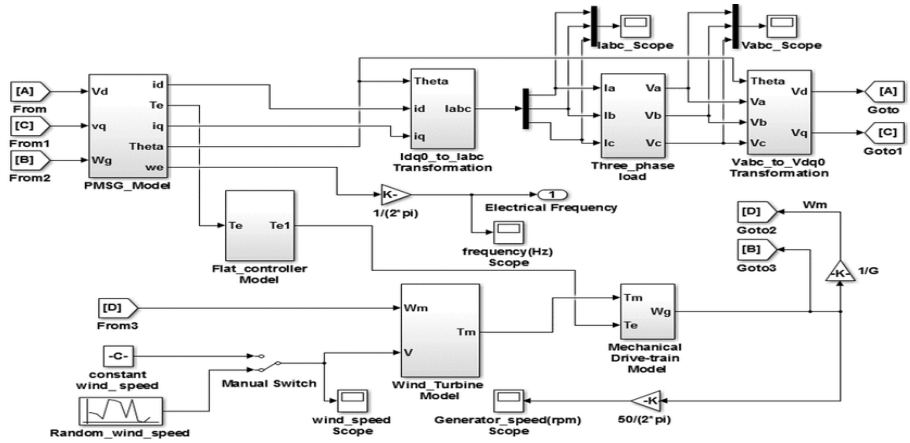

Fig. 8. Overall MATLAB simulink model of the system.

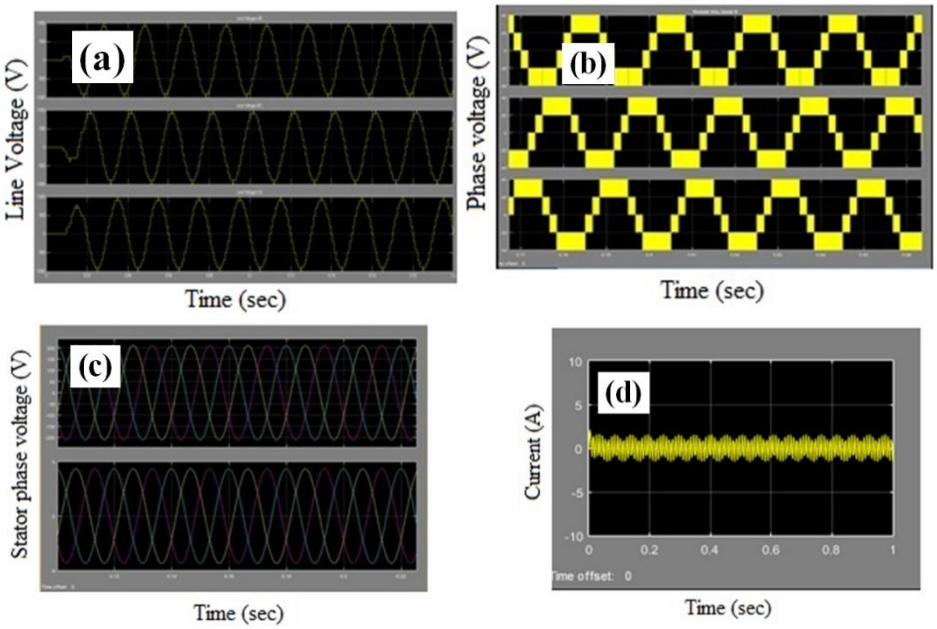

Fig. 9. Simulation outputs of the control block of the wind generation system, (a) response of low pass filter, (b) response of Inverter, (c) stator phase voltage, (d) stator output current per phase.

This technique gives the switching scheme of six power switches of three phase inverter. It uses six switching modes of the inverter to control the stator flux to approach the reference flux circle and attains higher control performance.

The switching states of the inverter are determined using the modulation technique. The modulation technique approximates the reference voltage by a combination of the six switching patterns. The stator voltage vectors can be chosen depending on the six

switching states of the inverter, and the simulation results of various outputs of the wind generation systems are shown in Fig. 9.

The ramp generator and ab angle sector output is given to the switch using a time calculator that generates gate timing signal to gates logic. From the gate logic circuit, the corresponding 6 gating signals are given to 6 switches. According to the gating signal of a switch, the inverter operates correctly and produces ac off signal, which is given to a second-order low-pass filter to get a pure sine waveform.

From the gate logic circuit, the corresponding 6 gating signals are given to 6 switches according to the gating signal of a switch, the inverter operates correctly and produces ac off signal, which is given to second order low pass filter to get a pure sine waveform as shown in Fig. 9(a) and the response of the inverter, stator phase voltage and stator output current per phase are shown in Fig. 9(b), 9(c) and 9(d) respectively.

5. Conclusion

The aim of receiving maximum power for wind turbine units in the power grid in the generation of electric power is one of the most important issues for modern wind turbine systems. In this research, the stator of a dual-feed induction generator is connected directly to the electric network system and rotor through transducers. The generator is controlled to tap the maximum energy from the wind, and the generator worked at its optimal point. The proposed minimization algorithm, initially, according to the generator power and speed, derived a relationship between d-axis current and the wind speed, which gives the optimum flux current reference to minimize the generator loss. In addition, fast transient responses have been obtained during the wind speed change. Since the wind turbine system runs at low wind speed most of the time, the proposed loss minimization algorithm is effective in increasing the output power from the generator. It is believed that this research work will serve as a suitable comprehensive reference for future research on Wind Turbine systems.

References

1. S. Joshi and K. M. Rao, J. Sci. Res. **12**, 233 (2020). http://dx.doi.org/10.3329/jsr.v12i3.42798
2. K. C. Kumar and K. Nagaraja, J. Sci. Res. **12**, 447 (2020). http://dx.doi.org/10.3329/jsr.v12i4.45182
3. F. Rong, L. He, S. Huang, C. He, X. Li, and C. Zhao, Sci. Rep. **12**, 19222 (2022). https://doi.org/10.1038/s41598-022-17761-4
4. H. D. P. Gonzalez and J. L. Dominguez-Garcia, Renew. Energy **187**, 248 (2022). https://doi.org/10.1016/j.renene.2022.01.046
5. A. Dalabeeh, A.-M. Anwar, T. M. Younes, A. Al-Rawashdeh, and A. Hindi, Bull. Elec. Eng. Inf. **9** (2020). https://doi.org/10.11591/eei.v9i2.1795
6. S. M. Suboh, M. S. Hassan, N. H. Baharudin, K. Ananda-Rao, N. B. Ahamad, E. C. Mid, M Othman, and J. Sardi, J. Phys. **1878**, ID 012045 (2021). https://doi.org/10.1088/1742-6596/1878/1/012045
7. A. Mesemanolis, C. Mademlis, and I. Kioskeridis, IEEE J. Power Electronics, **1**, 238 (2013). https://doi.org/10.1109/JESTPE.2013.2284562

8. Y. Wang, S. Wei, W. Yang, Y. Chai, and P. Li, Control Eng. Practice **127**, ID 105290 (2022). https://doi.org/10.1016/j.conengprac.2022.105290
9. A. G. Abo-Khalil, W. Alharbi, A. Al-Qawasmi, M. Alobaid, and I. Alarifi, J. Eng. Res. **13**, ID 2656 (2021). https://doi.org/10.3390/su13052656
10. M. G. Kebede and M. B. Tuka, J. Energy **22**, ID 8679053 (2022). https://doi.org/10.1155/2022/8679053
11. S. Zhou, F. Rong, and X. Ning, Energies, **14**, 4848 (2021). https://doi.org/10.3390/en14164848
12. J.-H. Liu and J.-S. Cheng, IEEE Transactions on Power System, **36**, 2729 (2021). https://doi.org/10.1109/TPWRS.2021.3053139
13. S. Siniscalchi-inna, F. D. Bianchi, M. De-Prada-Gil, and C. Ocampo-Martinez, Renew. Energy **131**, 37 (2019). https://doi.org/10.1016/j.renene.2018.06.112
14. S. Huang, Q. Wu, W. Bao, N. D. Hatziargyriou, L. Ding, and F. Rong, IEEE Transact. Sustanable Energy **12**, 25 (2021). https://doi.org/10.1109/TSTE.2019.2963549
15. C. Yang, S. Park, S. B. Lee, G. Jang, S. Kim, G. Jung, J. Lee, S. Shim, Y. K. Lim, and J. Kim, IEEE Ind. Appl. Magazine **25**, 69 (2019). https://doi.org/10.1109/MIAS.2019.2923105
16. F. Jiang, C. Tu, Q. Guo, Z. Wu, and Y. Li, IET Electr. Power Appl. **13**, 977 (2019). https://doi.org/10.1049/iet-epa.2018.5079
17. J. Ouyang, T. Tang, J. Yao, and M. Li, IEEE Transact. Energy Conversion **34**, 1501 (2019). https://doi.org/10.1109/TEC.2019.2905673
18. N. Karakasis, E. Tsioumas, N. Jabbour, A. M. Bazzi, and C. Mademli, IEEE Transact. Power Electronics **34**, 356 (2019). https://doi.org/10.1109/TPEL.2018.2823481